A double-porosity model for water flow in unsaturated concrete

Li, D; Li, L-Y; Wang, Xianfeng; Xing, Feng

Published in:
Applied Mathematical Modelling

DOI:
10.1016/j.apm.2017.09.022

Publication date:
2017

Applied Mathematical Modelling
Accepted 6 September 2017, Available online 14 September 2017
https://doi.org/10.1016/j.apm.2017.09.022

A double-porosity model for water flow in unsaturated concrete

Dawang Li[1], Long-yuan Li[2*], Xianfeng Wang[1*] and Feng Xing[1]
(1) Guangdong Provincial Key Laboratory of Durability for Maine Civil Engineering, Shenzhen University, Shenzhen 518060, P R China
(2) School of Engineering, University of Plymouth, Plymouth PL4 8AA, UK
(*) Coresponding authors (xfw@szu.edu.cn)

Abstract - This paper presents a double-porosity model for describing the moisture flow in unsaturated concrete. The two porosities used in the model represent the small pores of nano-scale and large pores of micro-scale, both of which are partially saturated with the moisture transport described by Darcy's law but with different transport properties. The model is applied to investigate the internal variation of saturation in a concrete in response to the change of humidity in the environment where the concrete is exposed. It is found that during wetting and drying cycles, the desaturation zone in concrete created in the first cycle expands continuously during the subsequent drying-wetting cycles. The wetting and drying cycles can push the desaturation zone from the surface layer into inner concrete gradually. This feature has not been explored in existing transport models.

Keywords: Double-porosity, moisture flow, unsaturated concrete, wetting, drying.

1. Introduction

Concrete is a porous material with pore sizes ranging from a few tenths of nanometres to several tens of micrometres. The concrete is referred to as a saturated concrete if the pores inside it are filled with water. Otherwise, it is called unsaturated concrete if the pores are occupied by water and air. When a concrete is subjected to wetting and drying cycles the degree of saturation of the pore space of the concrete can depend on different factors such as relative humidity and the previous exposure of the concrete to moisture. If the moisture content inside a concrete material is less than its saturation level, water may be absorbed into the concrete by large capillary forces arising from the contact of the very small pores of concrete with the liquid phase. This is an important mechanism of water flow into concrete, which is often observed in field applications subjected to wetting and drying cycles.

Existing experimental results have shown that the penetration of chloride ions in concrete subjected to wetting and drying cycles is considerably different from that in saturated environment [1]. It was also found that, due to the influence of water flow in concrete driven by wetting and drying the chloride diffusion profiles are quite different from those obtained in completely wetted concrete [2]. In literature the unsaturation effect on chloride penetration in concrete has been taken into account largely by modifying the diffusion coefficient of chlorides [3]. However, wetting and drying cycles can frequently change the degree of saturation of concrete and thus it is difficult and also not very accurate by simply employing a saturation-dependent chloride diffusion coefficient to predict the chloride penetration since, in most cases, the degree of saturation in a concrete is not uniform.

Efforts have been made to model the transport of both the water and chloride ions in concrete. For example, Wang *et al*. [4] developed a transport model of ionic solution and ionic species in an unsaturated concrete by considering the electrostatic interaction between different ionic species. Jin *et al*. [3] proposed a chloride transport model by taking into account the influence of both initial and surface saturation due to wetting and drying cycles. Emiko *et al*. [5] presented an experimental investigation into the factors affecting the sorption of water, chloride ingress and permeability of water into lightweight aggregate concrete. Bastidas-Arteaga *et al*. [6] proposed a probabilistic mathematical model for chloride penetration in unsaturated concrete using random variables to represent the model parameters, material properties, and stochastic processes to environmental actions. Sleiman *et al*. [7] presented a numerical model and the experimental validation on chloride transport in partially saturated concrete coupled with moisture transport in the concrete. Nguyen and Amiri [8] proposed a physical model of chloride ingress in concrete with consideration of electrical double layer in unsaturated concrete by solving multi-component ionic transport equations coupled with those of humidity. Wang and Ueda [9] presented a lattice network model based on the mesoscale composite structure of concrete to analyse the penetration property of concrete; especially the effects of microcracking induced by freeze-thaw damage on the unsaturated flow behaviour. Recently, Geng *et al*. [10] devloped a new, coupled transport model of ionic species and ionic solution in unsaturated concrete by taking into account the osmotic effect of ionic concentration on the transport of ionic solution due to the small pore sizes in concrete.

Note that all of the aforementioned transport models describing for water flow were developed based on the simplified assumption that the concrete pore system is macropores, which are partially saturated with transport driven by the gradient in the vapour pressure of pore water. In reality, however, the concrete pore system has varying pore sizes, ranging from nano-scale C-S-H (calcium silicate hydrates) gel pores to micro-scale capillary pores [11,12]. In addiiton, voids greater than capillary pores may also exist, either from unintentional entrapment of air during the mixing procedure or from intentional air-entrainment, which purposefully disperses air voids throughout the paste to relieve pressures induced from the freezing of water in pores. According to the physical thermodynamic models of condensation and adsorption, the behaviour of water flow in nano-sclae pore system will be significantly different from that in micro-scale pore system, not only because the smaller pores have larger capillary actions, but also because there is chemical bond effect on the small-size pore surface which makes water difficult move. Therefore, to better describe the overall transport behaviour of the moisture in unsaturated concrete, it is necessary to distigush the transport features of the micro- and nano-scale pores in concrete. In this paper, a double-porosity model is presented to describe the flow of moisture in unsaturated concrete. In the two porosities one represents the large pore system and the other represents the small pore system, both of which are partially saturated with the moisture transport described by Darcy's law but with differently defined transport properties. The interference of the two pore systems is described by an interflow between them.

2. Double-porosity transport model

The concept of the double-porosity was developed in early 1960s for modelling the flow of a single component in a single phase within a naturally fractured reservoir (see, for example, [13]). Later, the concept has been applied to water transport in dolostones [14, 15], ionic transport in soils [16], ionic solution flow in fractured rocks [17], modelling of groundwater flow [18], modelling of waste and contaminant transport in soils [19, 20], modelling of fluid

flow in pavement [21], modelling of chloride penetration in concrete [12], investigation of interaction between ordinary Portland cement and opalinus clay [22], and study of the characteristic behaviour of a permeable medium containing regions which contribute significantly to the pore volume of the system but negligibly to the flow capacity [23]. The mathematical derivation of the double-porosity model for general porous materials was provided in references [24,25]. Recently, the double-porosity model has been further applied to the acoustic modeling of perforated concrete [26] and the investigation of concrete creep induced by moisture flow [27]. The central to the double-porosity approach is the assumption that the medium can be separated into two distict pore systems, both of which are treated as homogeneous media with seprate hydraulic transport properties. However, the mass transports in the two systems are coupled by using a term charcterising the exchange of mass in response to the pressure difference in the two systems. The double-porosity medium is considered to be a superposition of these two systems over the same volume. Hence, macroscopically, the porous medium at any point in time and space is characterised by two mass contents, two flow velocities, and two pressures defined in the two systems, respectively [28-30].

Consider the moisture flow in a concrete, which is made of a microscopically inhomogeneous porous matrix filled with moisture. Let Ω be a representative elementary volume (REV) of the porous material and Ω_f be the volume occupied by the fluid phase in Ω, through which water and air are able to travel. The porosity of the porous material thus can be expressed as follows,

$$\phi = \frac{\Omega_f}{\Omega} \tag{1}$$

where ϕ is the porosity of the concrete. The pores are now divided into two pore groups according to their sizes, namely the small pores and large pores. The former represent the gel pores and the latter represents the capillary pores and large voids. Let Ω_{f1} and Ω_{f2} be the volumes of the small and large pores in Ω, respectively. Hence, $\Omega_f = \Omega_{f1} + \Omega_{f2}$. The porosity of the material can be also expressed as follows,

$$\phi = \frac{\Omega_{f1}}{\Omega} + \frac{\Omega_{f2}}{\Omega} = \phi_1 + \phi_2 \tag{2}$$

where ϕ_1 and ϕ_2 are the porosities of the small and large pores, respectively. Let Γ be the external surfaces of the REV Ω, and Γ_{f1} and Γ_{f2} be the external surfaces of Ω_{f1} and Ω_{f2}, respectively. For most porous materials the following relationship holds between volumetric ratio and external surface ratio in the REV,

$$\phi_i = \frac{\Omega_{fi}}{\Omega} = \frac{\Gamma_{fi}}{\Gamma} \qquad (i = 1, 2) \tag{3}$$

Assume that pores are connected not only within each group but also between the groups (see Fig. 1). This means that the moisture can transport not only within each group but also between the groups. Based on the mass conservation of moisture in each pore system the following equations can be obtained,

$$\frac{\partial(\phi_1 \rho_1)}{\partial t} = -\nabla \cdot (\phi_1 \rho_1 V_1) + R_{12} \qquad \text{in } \Omega_{f1} \tag{4}$$

$$\frac{\partial(\phi_2 \rho_2)}{\partial t} = -\nabla \cdot (\phi_2 \rho_2 V_2) - R_{12} \qquad \text{in } \Omega_{f2} \tag{5}$$

where ρ_1 and ρ_2 are the densities of the moisture in Ω_{f1} and Ω_{f2}, t is the time, V_1 and V_2 are the flow velocities of the moisture in Ω_{f1} and Ω_{f2}, and R_{12} in kg/(m^3-s) is the mass exchange rate of the moisture between the small and large pores. According to Darcy's law, the flow velocity of the moisture in a porous material can be expressed in terms of the water pressure. Hence, V_1 and V_2 can be expressed as follows,

$$V_i = -K_i \nabla P_{il} \qquad (i = 1, 2) \qquad (6)$$

where K_i in m^4/(N-s) is a constant defined as the hydraulic conductivity (which equals the permeability divided by the dynamic viscosity) and P_{il} is the water pressure in Ω_{fi} (or the partial pressures in the liquid phase of Ω_{fi}), which can be expressed as follows (see Fig. 2),

$$P_{il} = P_{ig} - P_{ic} \qquad (i = 1, 2) \qquad (7)$$

where P_{ig} is the partial pressure in the gas phase of Ω_{fi} and P_{ic} is the capillary pressure in Ω_{fi}. Assume that the air in the gas phase is the ideal gas, that is

$$P_{ig} = P_{atm} \qquad (i = 1, 2) \qquad (8)$$

where P_{atm}=101325 Pa is the standard atmosphere pressure. Assume the capillary pressure can be approximated as

$$P_{ic} = \alpha_i P_{atm}\left(e^{\beta_i(1-\theta_i)} - 1\right) \qquad (i = 1, 2) \qquad (9)$$

where α_i and β_i are the dimensionless constants that can be determined using experimental data, $\theta_i = \rho_i/\rho_w$ is the degree of saturation of Ω_{fi}, and ρ_w=1000 kg/m^3 is the density of water.

Fig. 3 shows a comparison of the proposed capillary pressure with those calculated using the empirical formula proposed by Baroghel-Bouny [31] and the ideal gas law [32]. It is noticed from the figure that the capillary pressure proposed here is slightly different from those proposed by Baroghel-Bouny [31]. This is mainly to avoid the numerical difficulty when it is nearly saturated. Substituting Eqs. (6)-(9) into (4) and (5), it yields,

$$\frac{\partial \theta_1}{\partial t} = \nabla \cdot \left(D_{\theta 1} \nabla \theta_1\right) + \frac{R_{12}}{\rho_w \phi_1} \qquad \text{in } \Omega_{f1} \qquad (10)$$

$$\frac{\partial \theta_2}{\partial t} = \nabla \cdot \left(D_{\theta 2} \nabla \theta_2\right) - \frac{R_{12}}{\rho_w \phi_2} \qquad \text{in } \Omega_{f2} \qquad (11)$$

where $D_{\theta i}$ in m^2/s is the moisture diffusivity in Ω_{fi} and in the present study it is expressed as follows,

$$D_{\theta i} = K_i \theta_i \frac{dP_{il}}{d\theta_i} = -K_i \theta_i \frac{dP_{ic}}{d\theta_i} = K_i \alpha_i \beta_i P_{atm} \theta_i e^{\beta_i(1-\theta_i)} \qquad (i = 1, 2) \qquad (12)$$

Eq.(12) indicates that the moisture diffusivity is a function of the degree of saturation. Its variation with the degree of saturation depends on the choice of β value. In literature, Eqs. (10) and (11) are called as Richards' equation [33]. In order to solve for θ_1 and θ_2 from Eqs. (10) and (11), one has to know the mass exchange rate of the moisture between the small and large pores. Assume that the mass exchange rate is proportional to the pressure difference of the two pore systems, that is

$$R_{12} = k_{12} \rho_w (P_2 - P_1) \qquad (13)$$

where k_{12} in m^2/(N-s) is the constant and P_i is the average pore pressure in Ω_{fi}. Physically, a zero value of k_{12} implies that there is no mass exchange between the two systems and thus the transport of moisture in the two pore systems is completely independent. An infinite value of k_{12} implies that the mass exchange between the two systems is such fast that the two systems are forced to have identical average pore pressure although they have different transport

coefficients. Note that, if the pore is not saturated the volume of Ω_{fi} will be occupied by both the water and air. Thus the average pore pressure in Ω_{fi} is expressed as follows (see Fig. 4)

$$P_i = (1-\theta_i)P_{ig} + \theta_i P_{il} \qquad (i = 1, 2) \qquad (14)$$

Substituting Eqs. (7)-(9) into (14), it yields,

$$P_i = P_{atm}\left[1-\alpha_i\theta_i\left(e^{\beta_i(1-\theta_i)}-1\right)\right] \qquad (i = 1, 2) \qquad (15)$$

Fig. 5 shows a comparison of the average pore pressures calculated using different models. Two dissimilarities can be observed from the figure. First, for region θ_i>0.6 the present average pore pressure is slightly higher than those in other three models. Secondly, for region θ_i<0.2 the present average pore pressure decreases with the increase of the saturation level, which is similar to the ideal gas law but opposite to the Baroghel-Bouny model [31]. Nevertheless, in overall, they are all similar. The coupled mass conservation Eqs. (10) and (11) can be used to calculate the degree of saturation θ_1 in Ω_{f1} and θ_2 in Ω_{f2}, in which the moisture diffusivities are defined by Eq.(12) and the mass exchange rate is defined by Eqs. (13) and (15), provided that the initial condition and boundary conditions for θ_1 and θ_2 are also known. Note that, although the interporosity flow coefficient used in the present study is assumed as a constant, in principle, it can be time-dependent or a function of other variables as discussed in other studies [34-36].

3. Simulation of moisture transport due to wetting and drying cycles

The aforementioned moisture transport model is now applied to investigate the internal variation of saturation in a concrete in response to the change of humidity in the environment where the concrete is exposed. In all of the numerical examples shown below, the concrete is assumed to be initially saturated. Thus the initial condition is expressed as

$$\theta_i = 1 \qquad (i = 1, 2) \qquad (16)$$

The concrete analysed herein is assumed to have a wall-liked geometry, in which its one dimension is much smaller than its other two dimensions. Thus, the moisture transport in concrete can be simplified into a one-dimensional problem only along its short length represented by x-axis. Assume the problem is also symmetric about the line of $x = l$ where l is the half dimension of the short length. Thus, the two boundary conditions of the degree of saturation can be expressed as follows,

$$-D_{\theta i}\left.\frac{\partial\theta_i}{\partial x}\right|_{x=0} = k_{si}(\theta_i - \theta_{env}) \qquad (i = 1, 2) \qquad (17)$$

$$-D_{\theta i}\left.\frac{\partial\theta_i}{\partial x}\right|_{x=l} = 0 \qquad (i = 1, 2) \qquad (18)$$

where k_{si} in m/s is the convective coefficient of moisture transfer on concrete surface and θ_{env} is the equivalent degree of saturation in the environment where the concrete is exposed. Note that, instead of using a direct saturation boundary condition, Eq. (17) employs a flux boundary condition. This is because the surface moisture concentration in the pore solution may not be exactly the same as the moisture concentration in the environment. It is obvious from Eq. (17) that, if $k_{si}\to\infty$ then $\theta_i\to\theta_{env}$. This indicates that Eq. (17) also includes the saturation boundary condition used in the traditional moisture flow models. It should be pointed out that the use of surface flux boundary condition is very common in the heat transfer analysis. For example, the surface temperature of a concrete member exposed to a fire is significantly different from the hot air temperature on the surface, although they are at

the same position. Thus, the use of the heat flux boundary condition is more accurate than the use of the temperature boundary condition [37].

All parameters used in the present numerical simulations are listed in Table 1. The two porosities representing the small and large pore groups are assumed to be ϕ_1 = 0.05 and ϕ_2 = 0.15, respectively. The reason for having this assumption is the consideration of interfacial transition zones (ITZs) and micro cracks, which are categorized to the large pores. The two constants (α_i and β_i) used to define the capillary pressures are based on the experimental data as demonstrated in Fig. 3. However, as the smaller the pores the larger the capillary pressure, $\alpha_1=2\alpha_2$ is assumed, indicating that the capillary pressure in the small pores is doubled up. The assumption of the hydraulic conductivities (K_1 and K_2) is based on the published experimental value of moisture diffusivity that varies from 10^{-13} to 10^{-11} m^2/s. Again, since the smaller the pores the larger the resistance to the water travel, $K_1=K_2/10$ is assumed. The convective coefficients ($k_{s1}=k_{s2}= 4.0\text{x}10^{-7}$ $m^2/(N\text{-}s)$) of moisture transfer are assumed purely based on the hypothesis that there will be a small difference between the surface moisture content and the environment moisture content. The coefficient used to describe the mass exchange rate ($k_{12}=1.0\text{x}10^{-16}$ $m^2/(N\text{-}s)$) between the small and large pores is arbitrarily assumed as there is no available data in literature.

The set of partial differential equations defined by Eqs.(10) and (11) are solved using the "pdepe" solver, a code built in Matlab software, which solves initial-boundary value problems for parabolic-elliptic partial differential equations in one space variable x and time t to modest accuracy [38]. Using the "pdepe" the user needs to write a script to define the functions involved in the partial differential equations and the initial and boundary conditions. The solution is obtained on the user defined spatial mesh and the results are output at user defined times. In the "pdepe" solver the time increment is automatically determined by the solver but the mesh is defined by the user. In general, the denser the mesh used, the more accurate the obtained results. However, in most cases when the mesh reduces to a certain size, the results will remain almost identical for any further reduction in the mesh size. This is normally achieved by using a trial and error method.

As numerical examples, three cases are considered herein for a concrete wall of thickness of 40 mm. Because of geometrical symmetry only a half of the wall is modelled, that is l = 20 mm. In all cases a mesh of 201 equally spaced points is chosen for the half of the wall thickness, which is demonstrated to be small enough to produce accurate results by the trial and error method. The first case is the constant drying, in which the equivalent degree of saturation in the environment is assumed to be θ_{env}= 0.15. Fig. 6 shows the internal variation of the degree of saturation in the concrete at four different times, in which Fig. 6a and Fig.6b are for the small and large pore systems, respectively, whereas Fig.6c is the superposition of the two systems. It can be seen from the figure that, during the constant drying process the moisture moves gradually from inside to its exposure surface. Initially, it moves very quickly because of large gradient there. But, after 12 hours, the movement becomes slow and the rate of the movement is found to decrease with the increased time. Because of the assumption used for the hydraulic conductivity, which is ten times smaller in the small pore system than in the large pore system, the moisture flow in the small pore system is expected to be much slow. However, owing to the influence of its large capillary pressure and the mass exchange between the small and large pores the actual flow speed of the moisture in the small pore system is only about a half of that in the large pore system. Also, it can be overserved from the overall moisture distribution profiles shown in Fig. 6c that, due to the use of two porosities, the overall saturation distribution is different from that in either Fig.6a or Fig.6b

and the saturation level of the concrete in Fig.6c is higher in the deep zone where the moisture transport takes place only in the large pores, but lower in the shallow zone where the moisture transport takes place in both the large and small pores.

The second and third cases are for the wetting (θ_{env}=1) and drying (θ_{env}= 0.15) cycles with a period of 24 hrs as shown in Fig.7. In the second case the change between the wetting and drying follows a rectangular pattern, whereas in the third case it follows a modified sine function pattern. The internal variation of the degree of saturation in the concrete in response to the wetting and drying cycles is shown in Fig.8 for case two and Fig.9 for case three, respectively. It can be seen from Fig.8 that the moisture distribution profiles after a drying period and after a wetting period are significantly different, but the two profiles after a drying (t=12 and t=36 hrs) or after a wetting (t=24 and t=48 hrs) are analogous. The former is similar to the pattern of diffusion curve as shown in Fig.6, whereas the latter is similar to the pattern of parabolic curve. It is interesting to notice that, although there is a wetting period before the second drying the moisture distribution curve after the second drying period moves forward, which indicates that the wetting period prior to the drying has limited effect on the transport of the inside moisture. This is demonstrated by the moisture distribution curve after the second wetting period (t=24 and t=48 hrs), which shows the moisture content reduces continuously (that is the desaturation zone expands further) after the second drying and second wetting periods. This implies that the drying and wetting cycles can create a "wave-like" movement of the moisture, which can propagate from the surface layer into the inner concrete. This feature has not been reported in literature.

Fig. 9 shows the internal variation of the degree of saturation in the concrete in response to the change of humidity in the environment which follows the sine function as plotted in Fig.7. The main features of Fig.9 are similar to those shown in Fig.8, and thus are not discussed further. Only difference is the transport speed of the moisture that is slightly slower in Fig.9 than in Fig.8. As a consequence of this, the desaturation zone is slightly squeezed in the space but expanded in its amplitude, which reflects the difference between the sudden changes and smooth changes in the humidity in the environment.

Fig.10 shows the variation of the degree of saturation in the concrete after the drying and wetting (described in case 3) action in 11, 21, 41, and 81 days. It can be seen from the figure that, under the action of a half day drying in each drying-wetting cycle the desaturation zone expands gradually from exposure surface into the inner concrete. Note that, before the desaturation zone reaches to the end boundary (l = 20 mm) the zero flux boundary condition imposed at the end boundary has no influence on the moisture transport. In this case the moisture distribution curve exhibits like a parabolic curve with a clear minimum point. After the desaturation zone reaches to the end boundary (approximately after 22 days exposure), the zero flux boundary condition provides a reflection to the moisture transport, leading the right side of the parabolic curve becomes more platen, while the left side of the parabolic curve remains a sharp decrease. It is anticipated from the pattern and tendency of the curves shown in Fig.10 for different times that, the moisture distribution curve will reach a steady-state. The steady-state curve will have a uniformly distributed moisture in the inner concrete and a reduction distribution in the surface layer (2~3 mm), the latter of which defines the convection zone of the concrete when it is subjected to drying and wetting cycles.

4. Conclusions

It is well-known that the porosity and pore size distribution can affect the transport of moisture and ionic species in concrete. In this paper we have presented a double-porosity model for describing the moisture transport in concrete. The model has been applied to investigate the internal variation of the degree of saturation in concrete in response to externally applied wetting and drying cycles. From the present study the following conclusions can be drawn:

- The use of two porosities distinguished by pore size together with the consideration of mass exchange between the two porosities can appropriately reflect the transport features of concrete. The model is more accurate in predicting the moisture flow in concrete in response to externally applied wetting and drying cycles.

- During wetting and drying cycles, the desaturation zone in concrete created in the first cycle expands continuously during the subsequent drying-wetting cycles. The wetting and drying cycles can push the desaturation zones from the surface layer into inner concrete.

- For the same amplitude and period, the faster the change from wetting to drying and/or from drying to wetting on the exposure surface of concrete, the quicker the transport speed of moisture and thus the wider of the desaturation zone in concrete.

Acknowledgement - The authors would like to acknowledge the financial support received from the National Natural Science Foundation of China (Grant No. 51520105012).

References

[1] Thomas MDA and Matthews JD. Performance of pfa concrete in a marine environment - 10-year results. Cement and Concrete Composites (2004) **26(1)**: 5-20.

[2] Jin W, Zhang Y and Lu Z. Mechanism and mathematic modeling of chloride permeation in concrete under unsaturated state. Journal of the Chinese Ceramic Society (2008) **36(10)**: 1362-1369.

[3] Saetta AV, Scotta RV and Vitaliani RV. Analysis of chloride diffusion into partially saturated concrete. ACI Materials Journal (1993) **90(M47)**: 441– 451.

[4] Wang Y, Li LY and Page CL. Modelling of chloride ingress into concrete from a saline environment. Building and Environment (2001) **40(1)**: 1573–1582.

[5] Emiko L, Wee TH and Tamilselvan T. Penetrability of lightweight aggregate concrete. Magazine of Concrete Research (2010) **62(3)**: 201-209.

[6] Bastidas-Arteaga E, Chateauneuf A, Sánchez-Silva M, Bressolette P and Schoefs F. A comprehensive probabilistic model of chloride ingress in unsaturated concrete. Engineering Structures (2011) **33(3)**: 720-730.

[7] Sleiman H, Ait-Mokhtar A, Amiri O and Loche JM. Chloride transport through unsaturated concrete: Chloride profile simulations and experimental validation. Magazine of Concrete Research (2012) **64(4)**: 351-359.

[8] Nguyen PT and Amiri O. Study of electrical double layer effect on chloride transport in unsaturated concrete. Construction and Building Materials (2014) **50**: 492-498.

[9] Wang L and Ueda T. Mesoscale modeling of chloride penetration in unsaturated concrete damaged by freeze-thaw cycling. Journal of Materials in Civil Engineering (2014) **26(5)**: 955-965.

[10] Geng J, Li LY and Wang Y. Modelling of chloride penetration in unsaturated concrete. Advances in Cement Research (2016) **28(1)**: 51–61.

[11] Li LY. A pore size distribution-based chloride transport model in concrete. Magazine of Concrete Research (2014) **66(18)**: 937-947.

[12] Li LY, Easterbrook D, Xia J and Jin WL. Numerical simulation of chloride penetration in concrete in rapid chloride migration tests. Cement and Concrete Composites (2015) **63**: 113-121.

[13] Barenblatt GI, Zheltov IP and Kochina IN. Basic concepts in the theory of seepage of homogeneous liquids in fissured rocks, J. Appl. Math. Mech. (1960) **24(5)**: 1286-1303.

[14] Benavente D, Martínez-Martínez J, Cueto N and García-del-Cura MA. Salt weathering in dual-porosity building dolostones, Engineering Geology (2007) **94(3/4)**: 215-226.

[15] Cueto N, Benavente D, Martínez-Martínez J and García-del-Cura MA. Rock fabric, pore geometry and mineralogy effects on water transport in fractured dolostones, Engineering Geoloy (2009) **107(1/2)**: 1-15.

[16] Mori Y and Higashi N. Controlling solute transport processes in soils by using dual-porosity characteristics of natural soils, Colloids and Surfaces A: Physicochemical and Engineering Aspects (2009) **347(1–3)**: 121-127.

[17] Beneš M and Krupička L. Weak solutions of coupled dual porosity flows in fractured rock mass and structured porous media, Journal of Mathematical Analysis and Applications (2016) **433(1)**: 543-565.

[18] Bishop PK, Jakobsen R, Gosk E, Lerner DN and Burston MW. Investigation of a solvent polluted industrial site on a deep sandstone-mudstone sequence in the UK. Part 1 - Site description and groundwater flow, Journal of Hydrology (1993) **149(1–4)**: 209-229.

[19] Helton JC, Anderson DR, Baker BL, Bean JE, Berglund JW, Beyeler W, Garner JW, Iuzzolino HJ, Marietta MG, Rechard RP, Roache PJ, Rudeen DK, Schreiber JD, Swift PN, Tierney MS and Vaughn P. Effect of alternative conceptual models in a preliminary performance assessment for the waste isolation pilot plant, Nuclear Engineering and Design (1995) **154(3)**: 251-344.

[20] Kuráž M, Mayer P, Havlíček V, Pech P and Pavlásek J. Dual permeability variably saturated flow and contaminant transport modeling of a nuclear waste repository with capillary barrier protection, Applied Mathematics and Computation (2013) **219(13)**: 7127-7138.

[21] Brunetti G, Šimůnek J, and Piro P. A comprehensive numerical analysis of the hydraulic behavior of a permeable pavement, Journal of Hydrology (2016) **540:** 1146-1161.

[22] Jenni A, Gimmi T, Alt-Epping P, Mäder U and Cloet V. Interaction of ordinary Portland cement and Opalinus Clay: Dual porosity modelling compared to experimental data, Physics and Chemistry of the Earth, Parts A/B/C (2017) (http://dx.doi.org/10.1016/j.pce.2017.01.004).

[23] Warren JE, Root PJ. The Behavior of Naturally Fractured Reservoirs. SPE J. (1963) **3(3)**: 245-255 (SPE-426-PA).

[24] Arbogast T, Douglas J and Hoknung U. Derivation of the double porosity model of single phase flow via homogenization theory, SIAM J. Math. Anal. (1990) **21(4)**: 823-836.

[25] Showalter RE and Walkington NJ. Micro-structure models of diffusion in fissured media. Journal of Mathematical Analysis and Applications (1991) **155(1)**: 1-20.

[26] Carbajo J, Esquerdo-Lloret TV, Ramis J, Nadal-Gisbert AV and Denia FD. Acoustic modeling of perforated concrete using the dual porosity theory, Applied Acoustics (2007) **115**: 150-157.

[27] Vlahinić I, Thomas JJ, Jennings HM and Andrade JE. Transient creep effects and the lubricating power of water in materials ranging from paper to concrete and Kevlar, Journal of the Mechanics and Physics of Solids (2012) **60(7)**: 1350-1362.

[28] Bazant ZP and Thonguthai W. Pore pressure in heated concrete walls: theoretical prediction. Magazine of Concrete Research (1978) **31(107)**: 67-76.

[29] Tenchev RT, Li LY and Purkiss. Finite element analysis of coupled heat and moisture transfer in concrete subjected to fire, Numerical Heat Transfer (Part A: Applications) (2001) **39(7):** 685-710.

[30] Tenchev RT, Li LY, Purkiss JA and Khalafallah B. Finite element analysis of coupled heat and mass transfer in concrete when it is in a fire, Magazine of Concrete Research (2001) **53(2)**: 117-125.

[31] Baroghel-Bouny V. Water vapour sorption experiments on hardened cementitious materials. Part II – essential tool for assessment of transport properties and for durability prediction, Cement and Concrete Research (2007) **37(3)**: 438-454.

[32] Noggle JH. Physical Chemistry (3rd Edition). Harper Collins College Publishers (1996), New York.

[33] Martys NS. Diffusion in partially saturated porous materials, Materials and Structures (1999) **32(8)**: 555-562.

[34] Ranjbar E, Hassanzadeh H, Chen Z. Effect of fracture pressure depletion regimes on the dual-porosity shape factor for flow of compressible fluids in fractured porous media. Advances in water resources (2011) **34(12)**: 1681-1693.

[35] Ranjbar E, Hassanzadeh H, Chen Z. One-dimensional matrix-fracture transfer in dual porosity systems with variable block size distribution. Transport in porous media (2012) **95(1)**: 185-212.

[36] Haddad AS, Hassanzadeh H, Abedi J. Advective-diffusive mass transfer in fractured porous media with variable rock matrix block size. Journal of contaminant hydrology (2012) **133:** 94-107.

[37] Purkiss JA and Li LY. Fire Safety Engineering, Design of Structures (3rd edition). CRC Press (2013), Oxford.

[38] Skeel RD, Berzins M. A Method for the spatial discretization of parabolic equations in one space variable. SIAM Journal on Scientific and Statistical Computing (1990) **11(1)**: 1-32.

Table 1. Parameters used in simulation

Parameter	**Small pores (*i* = 1)**	**Large pores (*i* = 2)**	**Unit**
Porosity, ϕ_i	0.05	0.15	-
Hydraulic conductivity, K_i	$5.0\text{x}10^{-20}$	$5.0\text{x}10^{-19}$	$m^4/(N\text{-}s)$
Coefficient in capillary pressure, α_i	90	45	-
Coefficient in capillary pressure, β_i	5	5	-
Convective coefficient of moisture transfer, k_{si}	$4.0\text{x}10^{-7}$	$4.0\text{x}10^{-7}$	m/s
Coefficient in mass exchange rate, k_{12}	$1.0\text{x}10^{-16}$		$m^2/(N\text{-}s)$
Initial condition, θ_i	1	1	-
Boundary condition at $x = 0$, θ_{env}	Defined in each example		-
Boundary condition at $x = l$, *flux*	0	0	m/s

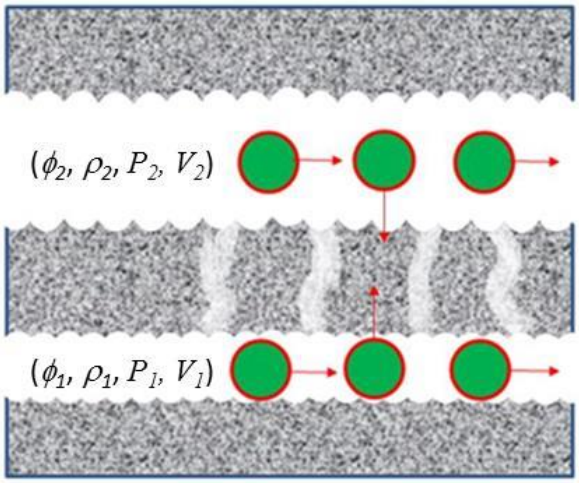

Fig.1 A schematic of moisture transport in two-porosity concrete (Green spheres: moisture, ϕ_k: porosity, ρ_k: density of moisture, V_k: flow velocity of moisture, P_k: average pore pressure).

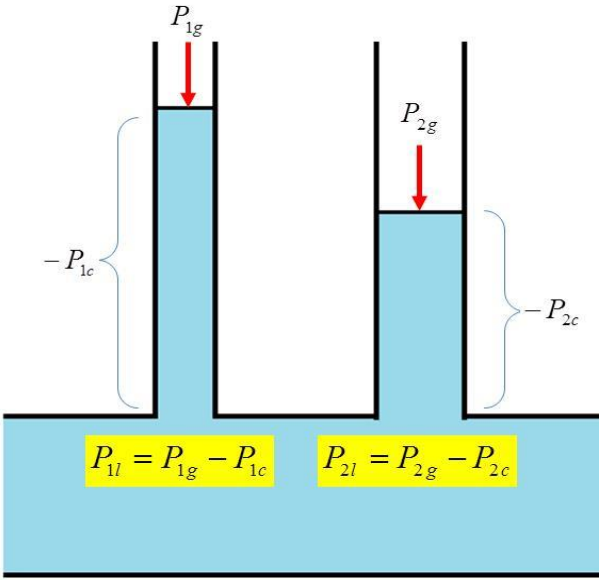

Fig.2 Liquid pressure in a partially saturated pore system (P_{ig}: partial pressure in gas phase, P_{il}: partial pressure in liquid phase, P_{ic}: capillary pressure, i = 1,2).

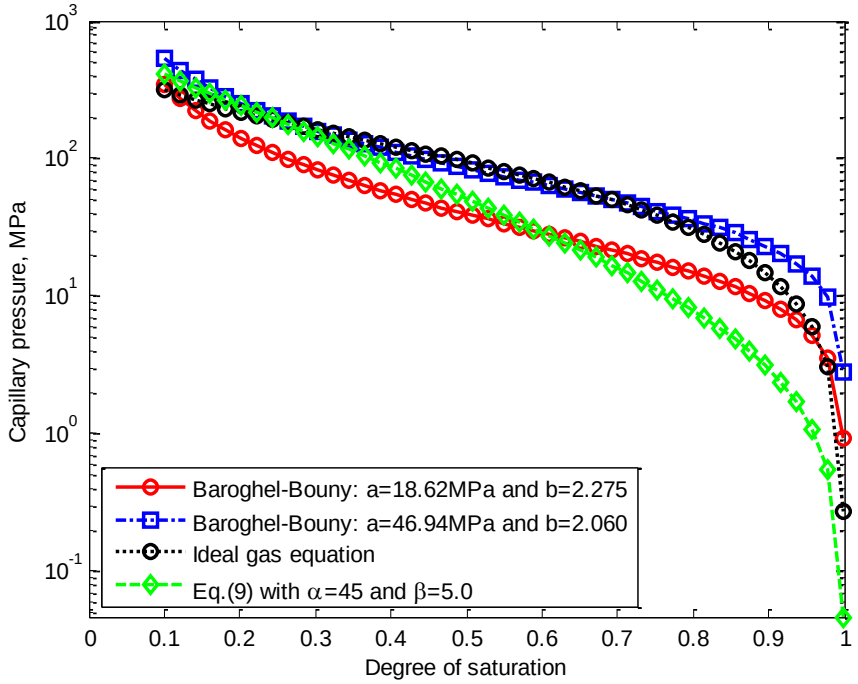

Fig.3 Comparison of capillary pressures calculated using different empirical formulas.

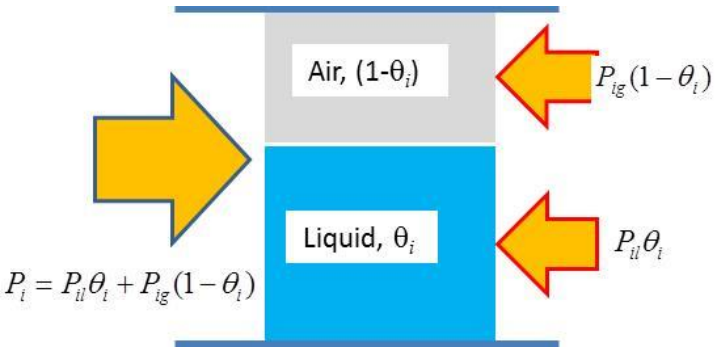

Fig.4 Average pore pressure in a partially saturated pore system (θ_i: degree of saturation, P_{ig}: partial pressure in gas phase, P_{il}: partial pressure in liquid phase, P_i: average pore pressure, i = 1,2).

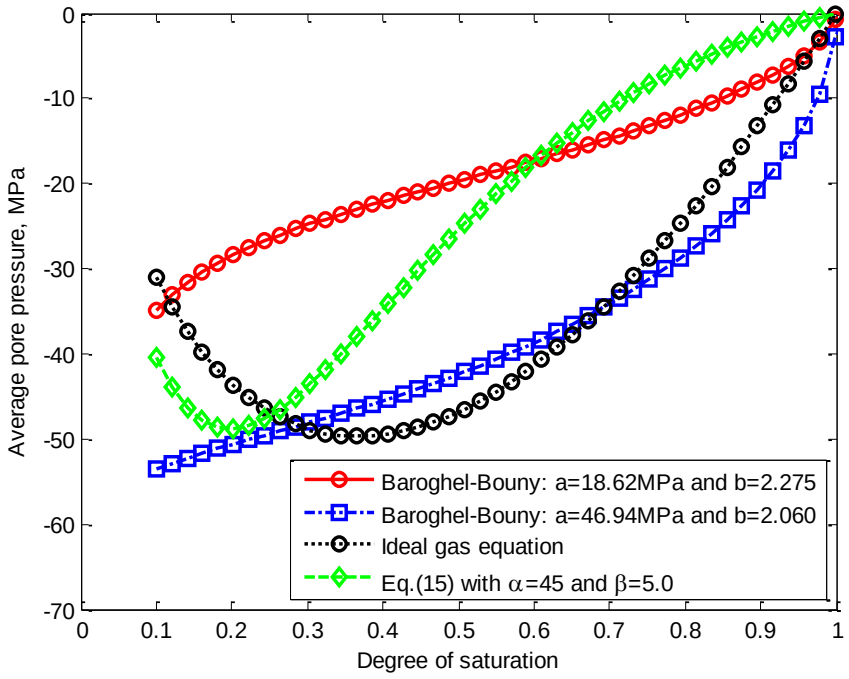

Fig.5 Comparison of average pore pressures calculated using different empirical formulas.

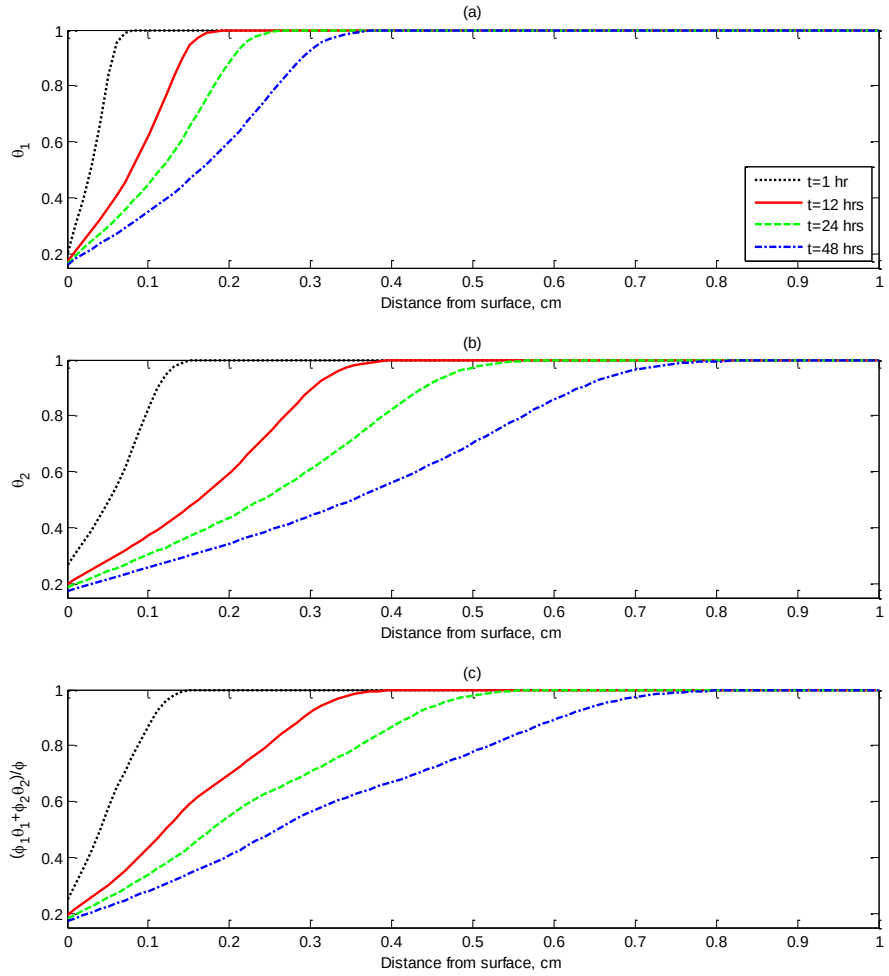

Fig.6 Variation of saturation during constant drying (case one) in (a) small pore system, (b) large pore system, and (c) overall pore system.

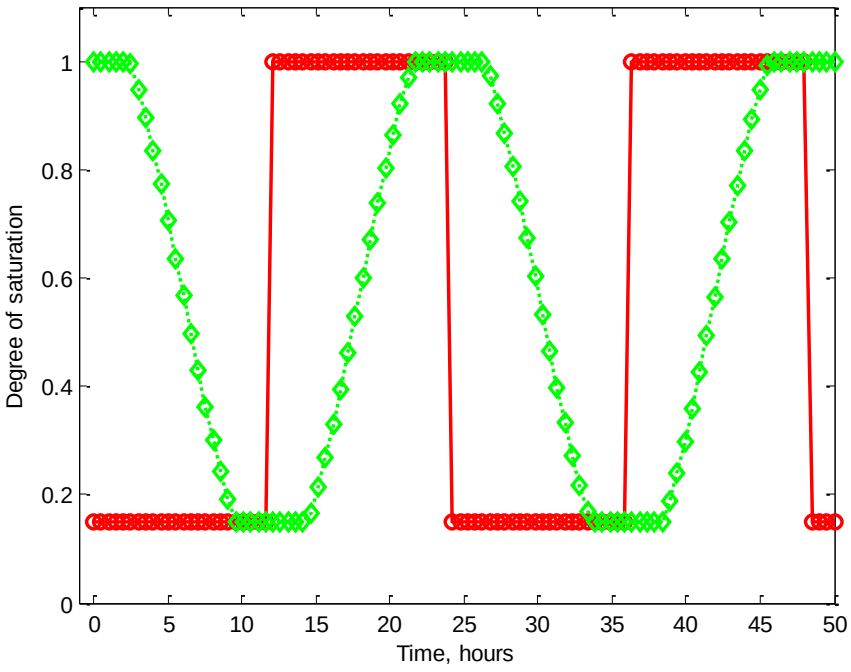

Fig.7 Surface saturation variation with time in wetting and drying cycles. Saturation varies from 0.15 to 1.0 with a period of 24 hrs. The rectangular variation (solid line) is for case two. The modified sine function (dash line) is for case three.

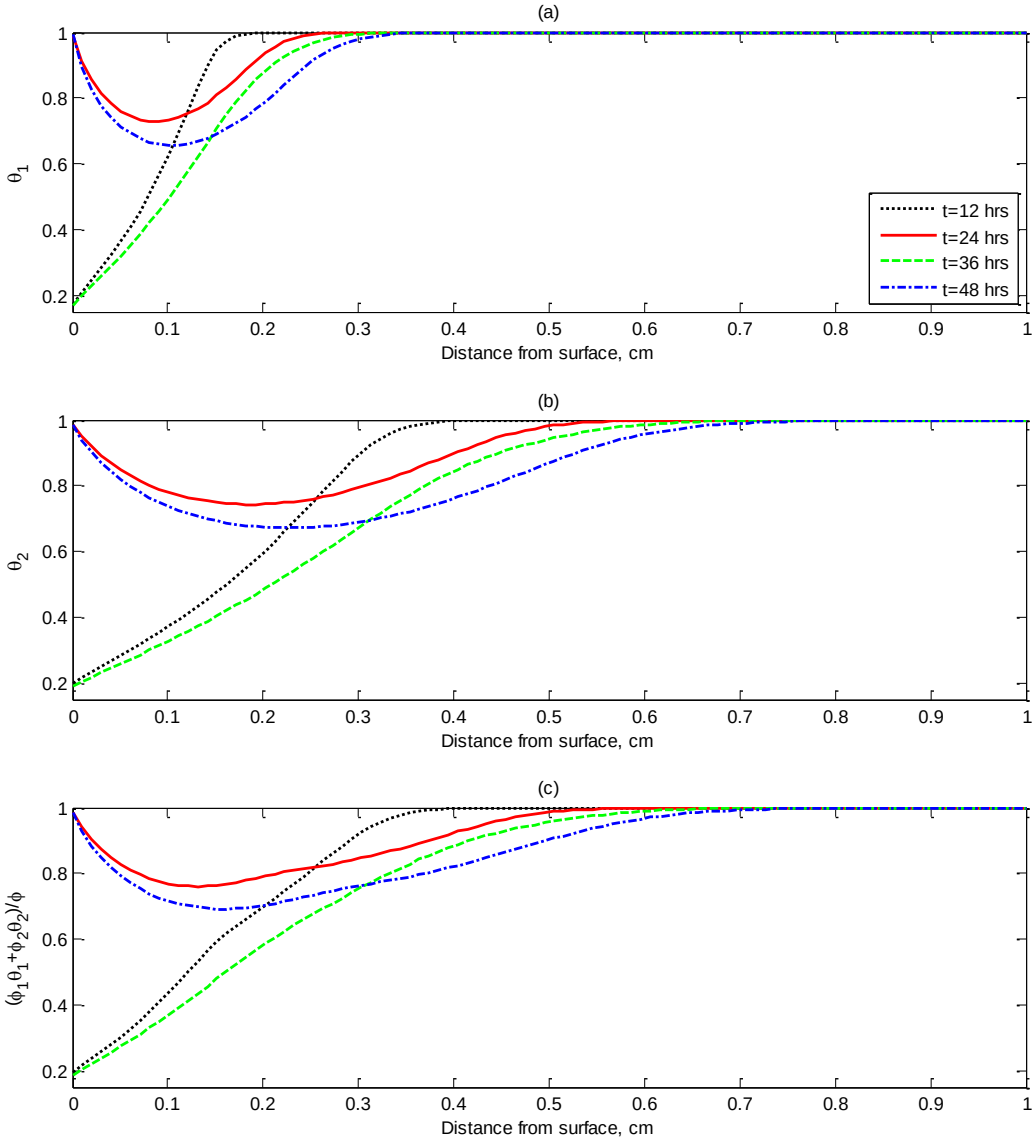

Fig.8 Variation of saturation during wetting and drying cycles (case two) in (a) small pore system, (b) large pore system, and (c) overall pore system.

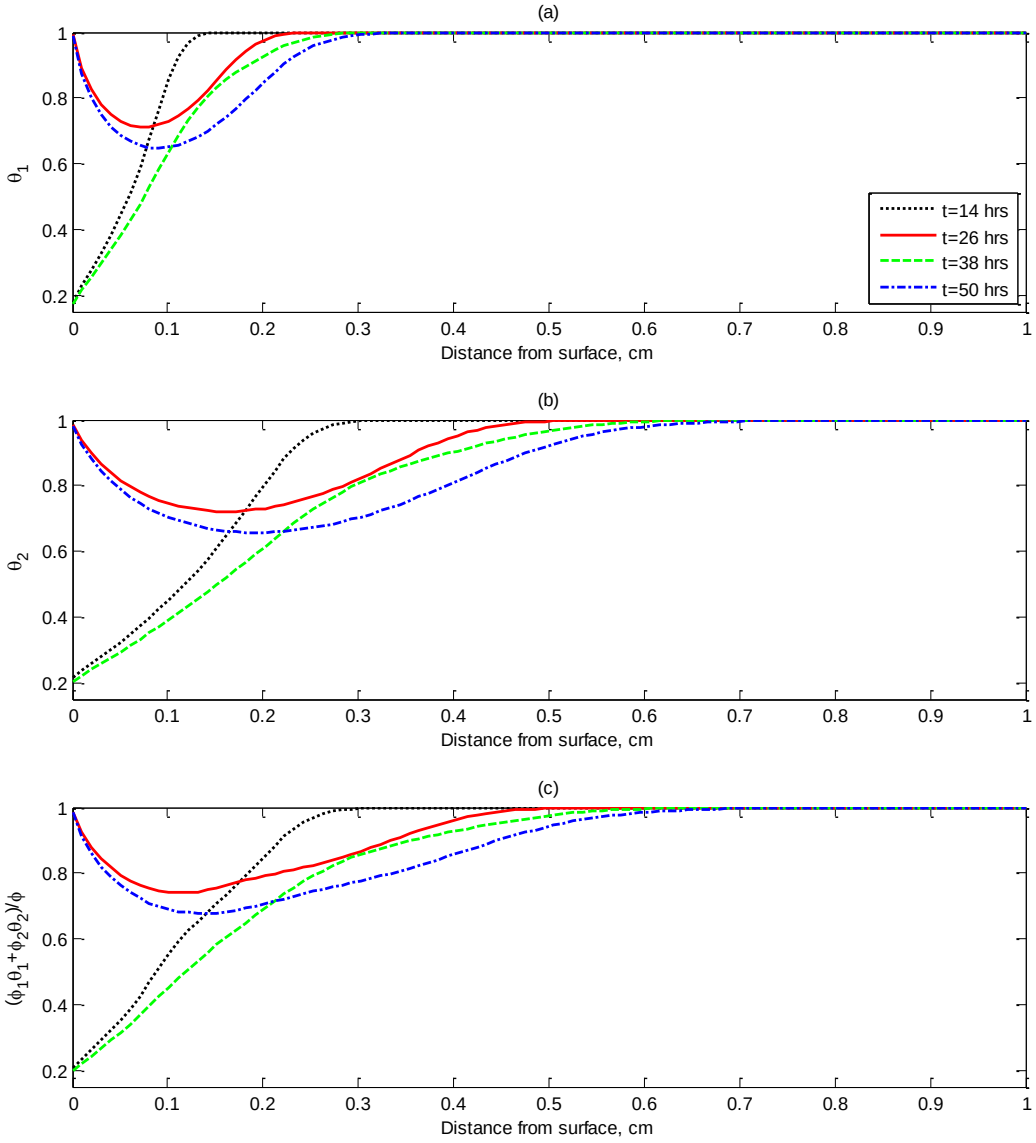

Fig.9 Variation of saturation during wetting and drying cycles (case three) in (a) small pore system, (b) large pore system, and (c) overall pore system.

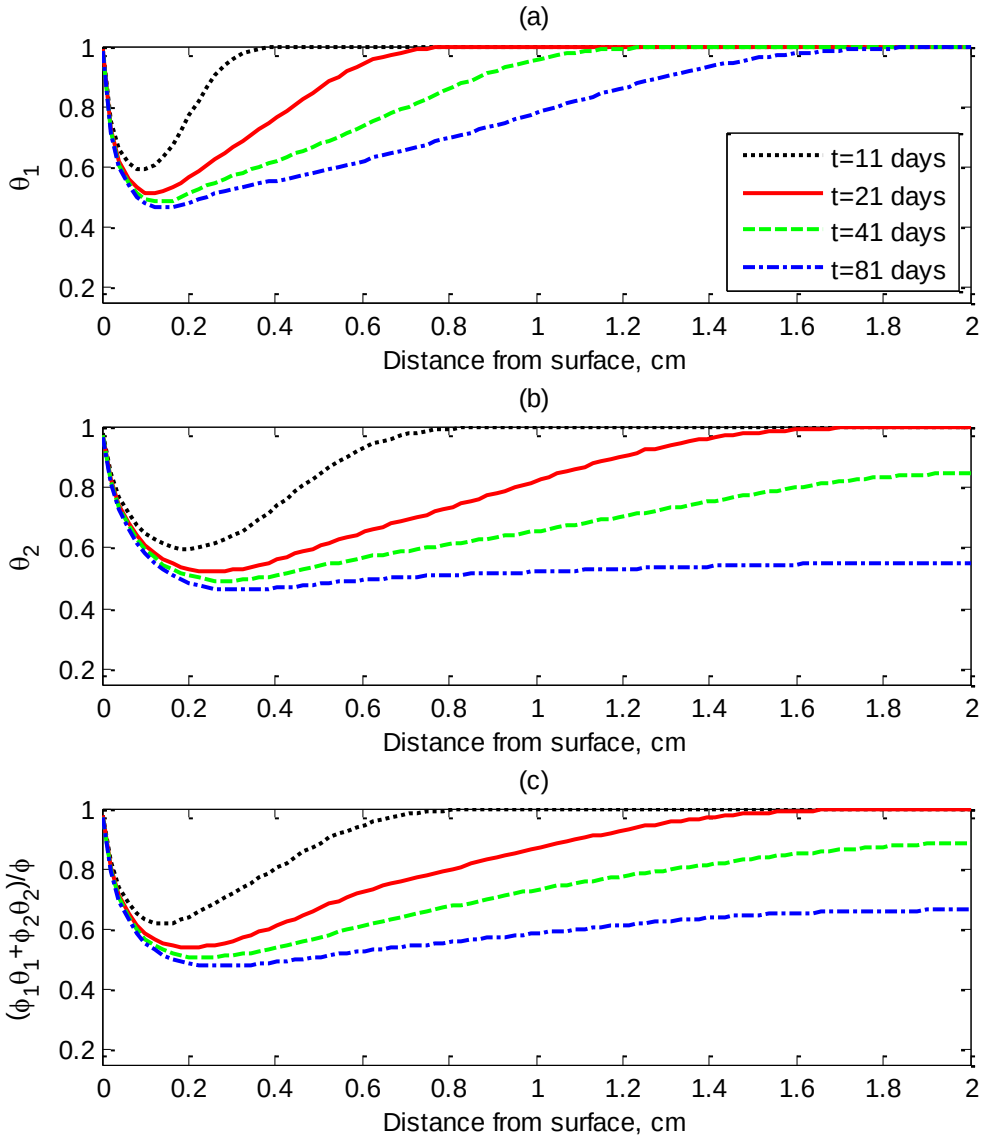

Fig.10 Variation of saturation during wetting and drying cycles (case three) in (a) small pore system, (b) large pore system, and (c) overall pore system on day 11, 21, 41 and 81 days.